Spectroscopic Demarcation of Emergent Photons and Spinons in a Dipolar-Octupolar Quantum Spin Liquid

Bin Gao,[1,2,*] Zhengbang Zhou,[3,*] Tingjun Zhang,[1,2,4] Andrey Podlesnyak,[5] Sang-Wook Cheong,[6] Yong Baek Kim,[3,†] and Pengcheng Dai[1,2,‡]

[1]*Department of Physics and Astronomy, Rice University, Houston, Texas 77005, USA*
[2]*Rice Laboratory for Emergent Magnetic Materials and Smalley-Curl Institute, Rice University, Houston, Texas 77005, USA*
[3]*Department of Physics, University of Toronto, Toronto, Ontario M5S 1A7, Canada*
[4]*Applied Physics Graduate Program, Smalley-Curl Institute, Rice University, Houston, Texas 77005, USA*
[5]*Neutron Scattering Division, Oak Ridge National Laboratory, Oak Ridge, Tennessee 37831, USA*
[6]*Keck Center for Quantum Magnetism and Department of Physics and Astronomy, Rutgers University, Piscataway, New Jersey 08854, USA*

(Received 23 December 2025; revised 12 March 2026; accepted 19 May 2026; published 23 June 2026)

The identification of fractionalized excitations in quantum spin liquids (QSLs) remains a central challenge in condensed matter physics. In dipolar-octupolar (DO) pyrochlores, such as $Ce_2Zr_2O_7$, the candidate π-flux quantum spin ice (QSI) state is predicted to host both gapless emergent photons and a continuum of spinons. However, resolving these modes at zero field is complicated by their spectral overlap and the presence of nonmagnetic scattering near zero energy. Here, we report neutron scattering experiments on $Ce_2Zr_2O_7$ under a magnetic field along the [1, 1, 1] direction. In contrast to previous unpolarized studies at zero field that relied on high-temperature subtraction, we use a same-temperature high-field subtraction protocol to isolate the photon and spinon modes. Leveraging the selective coupling of the magnetic field to the dipolar degrees of freedom, we demonstrate the spectroscopic demarcation of these excitations. We observe that weak fields ($\approx$0.15 T) suppress the low-energy photon weight while leaving the high-energy spinon continuum robust, albeit hardened. Our results, supported by gauge mean-field theory and exact diagonalization calculations, provide strong evidence for the π-flux QSI state and introduce a powerful field-tuning protocol for investigating DO-QSLs.

DOI: 10.1103/svt2-m3pp

Introduction—Quantum spin liquids (QSLs) are long-range entangled quantum phases of matter that support fractionalized excitations and emergent gauge structure [1–6]. Within this landscape, quantum spin ice (QSI) on the pyrochlore lattice is a three-dimensional quantum spin liquid that hosts an emergent U(1) lattice quantum electrodynamics with gapped bosonic spinons and linearly dispersing emergent photons [7–9]. The identification of a QSI in frustrated magnets has been an important goal in quantum spin liquid physics and frustrated magnets.

The cerium-based dipolar-octupolar (DO) pyrochlores, $Ce_2T_2O_7$ ($T = \mathrm{Sn, Zr, Hf}$), have recently emerged as leading candidate materials for realizing a U(1) quantum spin-ice (QSI) state [10–19]. These compounds exhibit no long-range magnetic order or spin-glass freezing down to tens of millikelvin, while inelastic neutron scattering (INS) reveals broad continua of spin excitations consistent with fractionalized dynamics despite comparatively weak structural disorder [10,12,14,15]. Their low-energy physics is governed by a well-isolated Ce^{3+} Kramers doublet, which can be described by pseudospin-1/2 operators $\tau^{x,y,z}$ [20,21] on the sites of the pyrochlore lattice. Under the D_{3d} point-group symmetry of the pyrochlore lattice, τ^x and τ^z transform as magnetic dipoles, whereas τ^y transforms as a magnetic octupole. In the corresponding gauge-theory description, the pseudospin component selected by the dominant exchange coupling plays the role of the emergent electric field, while the remaining pseudospin components generate dynamics of the conjugate gauge field. Microscopic analyses place $Ce_2Zr_2O_7$ specifically in the π-flux QSI regime, where the emergent gauge flux through hexagonal loops is π [14,19,22,23]. In this regime, the spinons display distinctive signatures, including a characteristic three-peak structure in the dynamical response [24,25], which has been extensively compared with INS measurements [8,12,19]. Moreover, additional quasielastic signals in the polarized neutron scattering and T^3 specific heat were interpreted as evidence for the emergent photons [26].

The central experimental challenge in separating the magnetic signal from the emergent photons at $E = \hbar\omega \approx 0$ meV [7,8,27] is the overlapping contributions from the strong nonmagnetic background scattering near the

*These authors contributed equally to this work.
†Contact author: yongbaek.kim@utoronto.ca
‡Contact author: pdai@rice.edu

 © 2026 American Physical Society

elastic line. Previous unpolarized neutron studies relied on high-temperature background subtraction to isolate magnetic signals, which assumes a temperature-independent background and nonmagnetic scattering [10–19]. While neutron polarization analysis can conclusively separate magnetic and nonmagnetic scattering [26], it suffers from poor statistics and is not readily compatible with the finite-field measurements, which is another way to investigate the magnetic field dependence of different degrees of freedom. These limitations motivate an alternative strategy for field-dependent INS spectroscopy.

In this Letter, we use a weak magnetic field along the [1, 1, 1] direction as a selective spectroscopic handle that enables a direct extraction of the emergent-photon signal. The key ingredient is the DO character of the Ce^{3+} Kramers doublet [20,28–30]. Since the projected magnetic moment within this doublet is carried solely by τ^z, a uniform magnetic field couples only linearly to τ^z, $H_{\mathrm{Zeeman}} = -\mu_B g_z \sum_i (\mathbf{H}\cdot\hat{\mathbf{z}}_i)\tau_i^z$, whereas the transverse sector is comparatively insensitive at linear order (equivalently, $g_\perp \approx 0$). This separation allows us to implement a same-temperature high-field background subtraction (STHFBS) protocol, in which the high-field spectrum at the base temperature serves as an internal reference. This contrasts with previous field-dependent INS studies for fields along the $[1, \bar{1}, 0]$ and [0, 0, 1] directions, which primarily tracked the suppression of the broad spinonlike continuum under strong polarization and did not directly resolve the gapless photon response [15,19]. In $Ce_2Zr_2O_7$, the predominantly Ising character of the ground-state doublet further suppresses conventional transverse fluctuations and thereby avoids field-induced ferromagnetic spin-wave branches, making the high-field state a clean reference for isolating intrinsic low-energy spin excitations. Applying STHFBS, we show that a modest [1, 1, 1] field efficiently suppresses the low-energy photon window while leaving the higher-energy continuum largely intact; subtracting the internal reference therefore isolates the fragile photon contribution from the robust spinon background. Combined with gauge mean-field theory (GMFT) and exact diagonalization (ED), this protocol provides independent and complementary spectroscopic evidence for the π-flux quantum spin-ice state [26].

Experimental methods—INS experiments were performed using the cold neutron chopper spectrometer (CNCS) at the Spallation Neutron Source (SNS). A large single crystal of $Ce_2Zr_2O_7$ (mass $\approx$2 g) was mounted on an oxygen-free copper holder (Supplemental Material, Fig. S1 [31]). The sample was cooled to a base temperature of $T \approx$ 50 mK using a dilution refrigerator equipped with a vertical-field cryomagnet, providing a magnetic field along the $[1, 1, 1]$ direction. Data were collected at incident neutron energy $E_i = 3.32$ meV under five distinct magnetic fields: $\mu_0 H = 0$, 0.1, 0.15, 0.2, and 3.0 T. All experimental results presented in this work are shown after subtracting the 3.0 T dataset as a background, effectively removing the field-independent nonmagnetic scattering. Full experimental details are provided in Supplemental Material (Figs. S2–S6) [31].

Theoretical calculations—We consider the most general nearest-neighbor model for DO pyrochlores [20,21], $\mathcal{H} = \sum_{\langle i,j\rangle,\alpha} \tilde{J}_\alpha \tau_i^\alpha \tau_j^\alpha + \sum_{\langle i,j\rangle} \tilde{J}_{xz}(\tau_i^x\tau_j^z + \tau_i^z\tau_j^x) - g_{zz}\mu_B \sum_i (\mathbf{H}\cdot\hat{\mathbf{z}}_i)\tau_i^z$, with $\alpha \in \{x, y, z\}$. A rotation of the pseudospins about the local y axis by an angle θ, $\tau_i^y = S_i^y$, $\tau_i^x = \cos\theta S_i^x - \sin\theta S_i^z$, $\tau_i^z = \sin\theta S_i^x + \cos\theta S_i^z$, diagonalizes the (x, z) sector, with $\tan(2\theta) = (2\tilde{J}_{xz}/\tilde{J}_x - \tilde{J}_z)$, thereby eliminating the mixed $\tau_i^x\tau_j^z$ terms and yielding an XYZ Hamiltonian

$$\mathcal{H} = \sum_{\langle i,j\rangle,\alpha} J_\alpha S_i^\alpha S_j^\alpha + \mathcal{H}_{\mathrm{Zeeman}}, \tag{1}$$

where $\mathcal{H}_{\mathrm{Zeeman}} = -\mu_B \sum_i g_{zz}(\mathbf{H}\cdot\hat{\mathbf{z}}_i)(\cos\theta S_i^z + \sin\theta S_i^x)$. Crucially, θ has direct physical content. When $\tilde{J}_{xz} \neq 0$, the exchange eigenmodes (S^x, S^z) are rotated relative to this dipole axis, so the physical magnetization operator is $\tau^z = \cos\theta S^z + \sin\theta S^x$. Thus, θ controls how experimental probes partition spectral weight between S^z and S^x channels. In this sense, θ quantifies the dipole-octupole hybridization and sets the degree of channel mixing visible in field-dependent spectroscopy.

For $Ce_2Zr_2O_7$, we adopt the experimentally motivated parameters $(J_{xx}, J_{yy}, J_{zz}, \theta) = (0.063\ \mathrm{meV}, 0.062\ \mathrm{meV}, 0.011\ \mathrm{meV}, 0.2\pi)$ [14,19]. Here, we choose a larger θ compared with the best fit parameters from experiments for reasons discussed in Supplemental Material [31]. With these parameters, the model lies in the QSI regime [3,7,8,24,25,27,38–47]. In direct analogy with U(1) gauge theory, $S^x \sim E$ is the emergent electric field, while the transverse operators $S^\pm \sim S^y \pm iS^z \sim \Phi^\dagger e^{\pm iA}\Phi$ implement spinon Φ hopping in the background gauge field A [1,25,45,48–52].

As neutron spins couple only to the dipolar component τ^z, the neutron-scattering cross section is proportional to the $\langle\tau^z\tau^z\rangle$ correlation function. In the S^α basis, $\langle\tau^z\tau^z\rangle = \sin^2\theta\langle S^xS^x\rangle + \cos^2\theta\langle S^zS^z\rangle + \sin(2\theta)\mathrm{Re}\langle S^xS^z\rangle$. These three terms correspond, respectively, to the photon, spinon, and photon-spinon mixing channel. We can evaluate the corresponding dynamical correlations using ED on a 16-site conventional cubic pyrochlore cluster with periodic boundary conditions [53–57].

Results and spectral demarcation—(i) Photon sector ($E < 0.05$ meV):At zero field, this window is dominated by a gapless, linearly dispersing photon mode [7,8,58]. Upon applying $\mathbf{H}\|[1, 1, 1]$, the intensity in this window is rapidly depleted [59] and is nearly extinguished by $\|\mu_0\mathbf{H}\| = 0.15$ T. Since GMFT places the confinement transition at larger fields [60], we attribute this apparent “gapping” not to photon confinement, but to a field-induced redistribution of photon-dominated weight: the field introduces a mixing channel that strongly suppresses

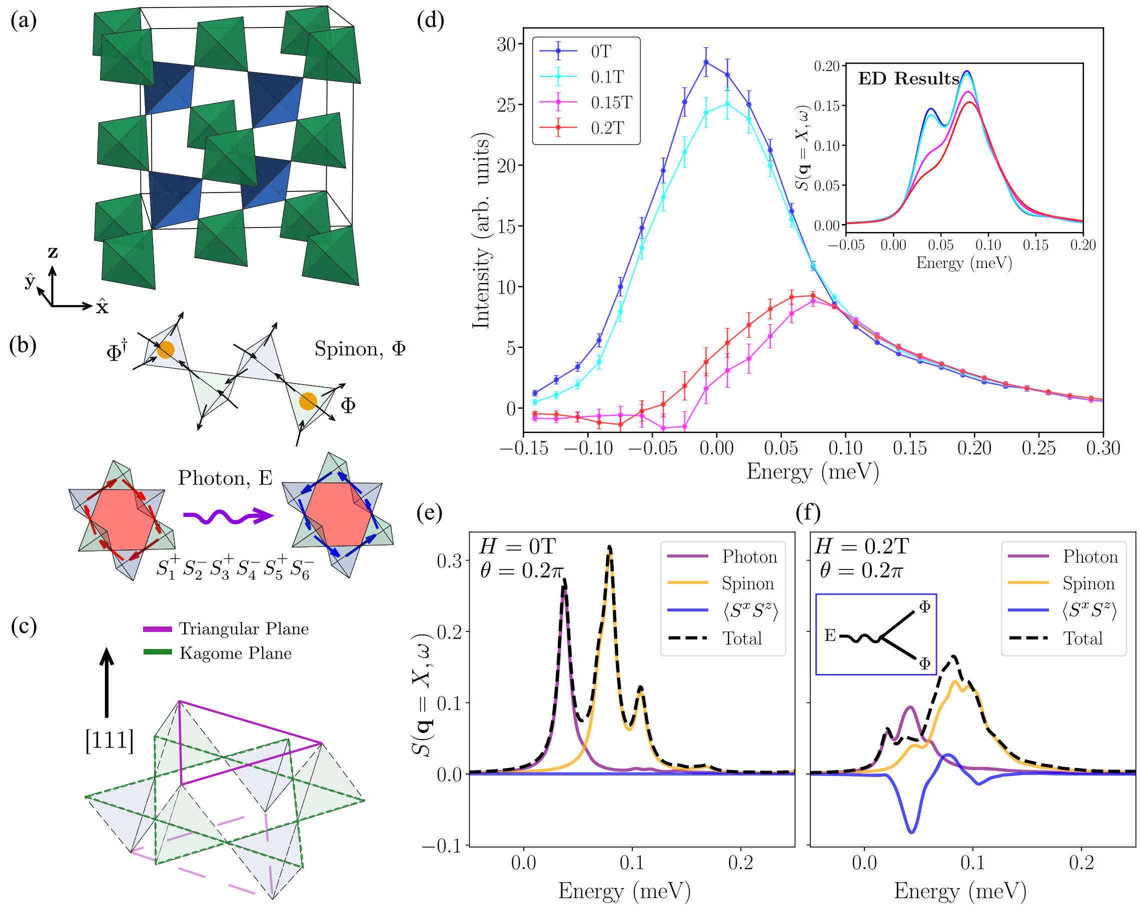

FIG. 1. (a) Pyrochlore network of Ce^{3+} ions (corner-sharing tetrahedra) viewed along a cubic axis. (b) Spinon and photon sectors under a $[1,1,1]$ field. A gapped bosonic spinon Φ propagates on the dual diamond lattice formed by tetrahedron centers, with $\Phi^\dagger$ and Φ denoting creation and annihilation of gauge charges (orange circles) on opposite sublattices. The emergent photon E corresponds to transverse fluctuations of the U(1) gauge field on the six bonds of a pyrochlore hexagon; in the rotated local DO basis this is represented by the bond operator product $S_1^+S_2^-S_3^+S_4^-S_5^+S_6^-$, whose two circulation senses (red and blue arrows) give $\pm E$ excitations. (c) Decomposition of the pyrochlore lattice into kagome planes (green) and triangular planes (magenta) stacked along the global $[1,1,1]$ direction (black arrow). (d) Energy dependence of the momentum-integrated intensity in the first Brillouin zone of $Ce_2Zr_2O_7$ at $T\approx 50$ mK, after subtracting the same-temperature 3.0 T dataset as a high-field background. Curves show data for $||\mu_0\mathbf{H}|| = 0, 0.10, 0.15, 0.20$ T (blue, cyan, magenta, red), integrated over the full $([H,-H,0],[H,H,-2H])$ plane excluding a region near the Γ point. At zero field, a pronounced low-energy peak below $\sim$0.05 meV reflects the emergent photon mode; with increasing field, this peak is rapidly suppressed, while the higher-energy tail above $\sim$0.10 meV remains comparatively unchanged. Inset: ED results for $S(\mathbf{q}=X,\omega)$ of the DO U(1) QSL convolved with a Gaussian filter to emulate experimental resolution for the same set of fields, demonstrating convincing qualitative agreement. (e) ED calculation of the dynamical structure factor at the X point, $S(\mathbf{q}=X,\omega)$, in zero field $H=0$ for a representative mixing angle $\theta=0.2\pi$. The total neutron response (black dashed) is decomposed into contributions from the emergent photon mode (purple), gapped spinon excitations (gold), and the photon-spinon mixing $\langle S^xS^z\rangle$ (blue). The dominant low-energy peak arises from the photon, while the spinon continuum lies at higher energy. (f) Same as (e) but in a finite $[1,1,1]$ field $H=0.2$ T. The inset illustrates the corresponding GMFT vertex of the mixed correlator $\langle S^xS^z\rangle$. This vertex hybridizes the photon and spinon sectors, enabling a field-tunable redistribution of spectral weight between photon and spinon channels that underlies our experimental disentanglement scheme.

the spectral weight of the quasielastic window. We elaborate on these mechanisms below.

A uniform $[1,1,1]$ field couples differently to the four pyrochlore sublattices because their local axes $\hat{\mathbf{z}}_i$ are inequivalent. The Zeeman term $\mathcal{H}_{\mathrm{Zeeman}}$ therefore naturally decomposes the lattice into alternating kagome and triangular layers [Fig. 1(b)]. As shown in Ref. [61], this lowered symmetry splits the photon dispersion into two branches already at leading order, producing a broader low-energy response. Consistent with this expectation, our ED results show that the sharp quasielastic photon peak at $\mathbf{H}=0$ [Fig. 1(e)] evolves into a broadened low-energy structure at $||\mu_0\mathbf{H}|| = 0.2$ T (still below the critical field) [Fig. 1(f)].

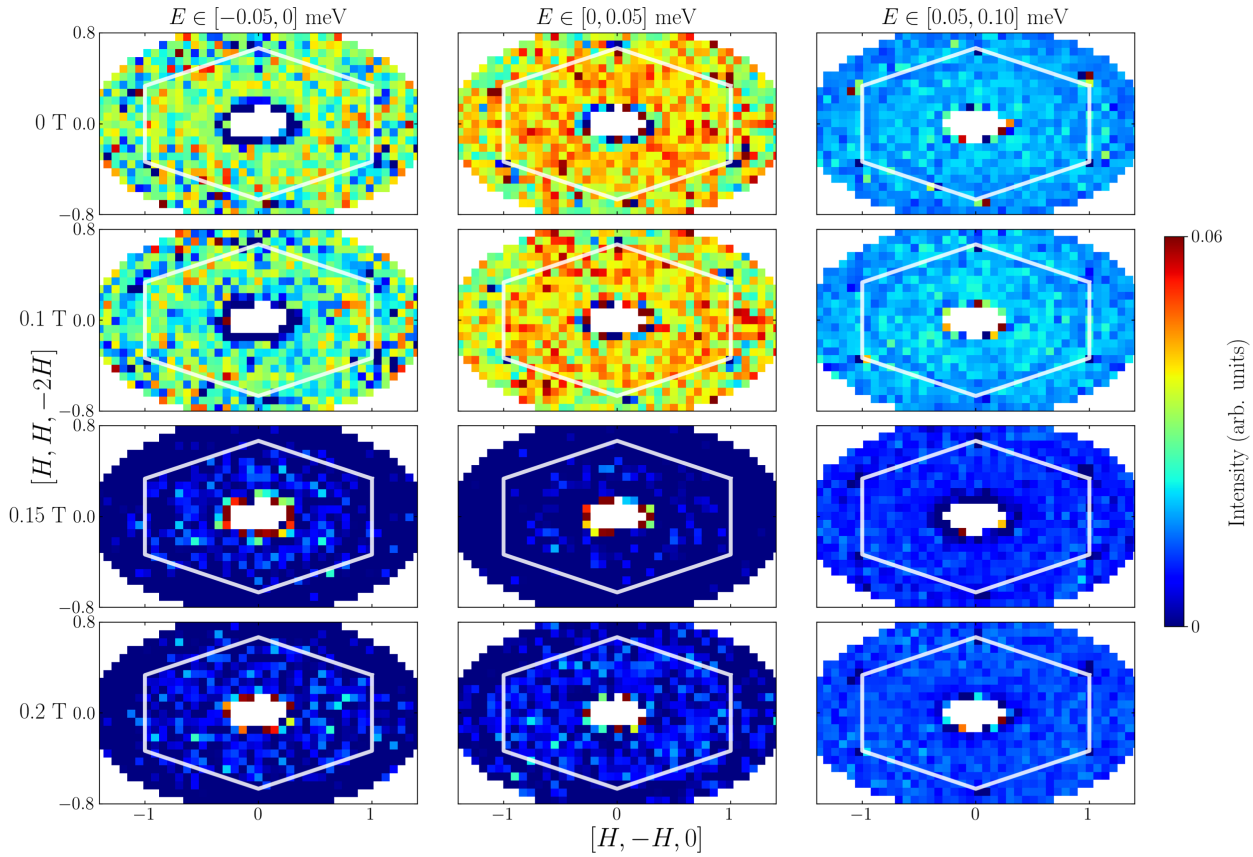

FIG. 2. Field and energy evolution of low-energy neutron scattering in $Ce_2Zr_2O_7$. Constant-energy slices of $S(\mathbf{Q}, \omega)$ in the $([H, -H, 0], [H, H, -2H])$ plane at $T \simeq 50$ mK, shown for $H = 0$, 0.10, 0.15, and 0.20 T (rows). For each field, the same-temperature 3.0 T dataset is subtracted to reduce field-independent nonmagnetic background. Columns correspond to the energy-integration windows $E \in [-0.05, 0]$, [0, 0.05], and [0.05, 0.10] meV (left to right). Hexagons indicate the boundary of the Brillouin zone of the pyrochlore lattice in these reciprocal-lattice units. To avoid a known instrumental feature identified from a vanadium measurement, data are displayed only within an elliptical region of interest corresponding to $|\mathbf{Q}| < 1.25$ Å^{-1} (see Fig. S6 of Supplemental Material for the full Q map [31]). The first two columns (near-elastic window) emphasize the low-energy response discussed in the text as photon dominated, which is rapidly suppressed with field, while the 0.05–0.10 meV window highlights residual continuum spectral weight that persists to higher fields.

A key consequence of $\mathbf{H} \| [1, 1, 1]$ is that it turns on a spinon-photon mixing channel that selectively modifies the quasielastic response. At $\mathbf{H} = 0$, the mixed correlator $\langle S^x S^z \rangle$ vanishes, enforced by $\mathbb{Z}_2$ symmetries corresponding to independent π rotations that flip S^x or S^z. For $\theta \neq 0$, the Zeeman term couples to a linear combination of S^x and S^z, explicitly breaking these $\mathbb{Z}_2$ symmetries and permitting $\langle S^x S^z \rangle \neq 0$. The resulting hybridization strongly suppresses photon-dominated spectral weight for $E \lesssim 0.05$ meV [Fig. 1(f)], producing an apparent low-energy "gap" in the neutron response even when the applied field remains below the true confinement transition expected from GMFT [60]. With this mechanism included, the ED spectrum [Fig. 1(d)] quantitatively reproduces the experimental line shape. For comparison to experiment, we use $S(\mathbf{q} = X, \omega)$ as a practical proxy for the momentum-integrated inelastic response. Empirically, all wave vectors away from Γ and the magnetic Bragg positions exhibit a rapid depletion of the quasielastic photon-window intensity. We therefore take X as a representative point. This choice is also directly validated by the data: restricting the analysis to the CNCS-accessible X-equivalent patch yields the same qualitative agreement between ED and experiment (Fig. S4 of Supplemental Material [31]).

The integrated-intensity analysis [Fig. 1(d)], together with the momentum-resolved spectra (Fig. 2), indicates a reorganization of low-energy spectral weight under field rather than a uniform attenuation. As $\|\mu_0 \mathbf{H}\|$ increases, the inelastic intensity in the photon window, integrated over the first Brillouin zone but excluding a small region around Γ, is strongly depleted. Within this restricted (Q, ω) window, the suppressed weight is not recovered in the measured inelastic response away from Γ, implying a transfer into channels not included in the integral. In particular, consistency with neutron-scattering sum rules suggests that the missing low-energy weight is redistributed primarily into

(i) the excluded near-Γ region and/or (ii) the elastic (Bragg) channel at reciprocal-lattice vectors as field-induced static correlations grow (and possibly into energies outside the plotted photon window). This interpretation is supported by the observed enhancement of quasielastic-elastic intensity near the magnetic Bragg position $(2, -2, 0)$ (Fig. S5 of Supplemental Material [31]) and by the ED results (Fig. S8 of Supplemental Material), which likewise show increased low-energy weight at these momenta at finite fields.

(ii) Spinon sector (0.05 meV $< E < 0.10$ meV):In this intermediate window, the intensity decreases with field but does not vanish. This reduction is consistent with field-induced reshaping of the low-energy spectrum: broadening shifts part of the lower spectral edge toward $E \lesssim 0.05$ meV (where it is further suppressed by the mixing mechanism), while a robust residual signal persists up to $\|\mu_0 \mathbf{H}\| = 0.2$ T, which we associate with the gapped spinon continuum that remains dynamically active in this field range [60,62].

(iii) High-energy background ($E > 0.15$ meV):This region shows negligible magnetic intensity across all fields after subtraction (see Fig. S6 of Supplemental Material for details [31]), providing an internal consistency check for the background-removal procedure.

Finally, we validate the subtraction protocol by comparing our zero-field integrated intensity with the magnetic [Fig. 1(d)] spectral weight isolated via polarized neutron scattering in Ref. [26]. Both methods yield the same characteristic energy dependence—a sharp low-energy photon feature followed by a broader continuum—demonstrating that same-temperature high-field subtraction reliably recovers the intrinsic magnetic spectrum and provides a practical alternative to polarized setups for DO pyrochlores (Supplemental Material, Fig. S3).

Discussion—Previous unpolarized neutron-scattering studies often attempted to extract the photon signal by subtracting a high-temperature dataset (typically $T \approx 12$ K), assuming that the nonmagnetic background is essentially temperature independent between base temperature and 12 K, while the magnetic response at elevated temperature is diffuse and nearly energy independent. As discussed in Ref. [26], this assumption breaks down in the low-energy window relevant for the emergent photon. The Bose population factor strongly enhances bosonic contributions below ~1 meV at 12 K, including phonons and other quasielastic background scattering, whereas these contributions are strongly suppressed at base temperature. Consistently, the integrated intensity at the elastic line is found to be larger at 12 K than at $T \approx 30$ mK over much of reciprocal space, indicating substantial thermally induced quasielastic weight. As a result, high-temperature subtraction leads to systematic oversubtraction of the near-elastic signal and can remove precisely the low-energy magnetic response of interest. Recent polarized-neutron and heat-capacity measurements on $Ce_2Zr_2O_7$ circumvented this difficulty and provided evidence consistent with an emergent-photon contribution [26]. However, neutron polarization analysis is not readily compatible with the finite-field geometry required here: the external field at the sample overwhelms the small guide field used to define the neutron spin quantization axis, and the reduced flux of polarized triple-axis measurements further limits systematic field-dependent studies.

By contrast, our STHFBS protocol avoids these limitations by using the base-temperature high-field spectrum as an internal reference. The key observation is the sharply different field evolution of the two low-energy components: a fragile, photon-dominated quasielastic response that is rapidly suppressed by field, and a higher-energy spinon continuum that remains comparatively robust. This separation in field response provides a direct fingerprint of the composite QSI spectrum in which the photonic signature can be reliably isolated. Such dichotomous behavior is difficult to reconcile with a conventional magnon scenario, but follows naturally from the fractionalized gauge–spinon structure of the π-flux QSI state.

Conclusion—We show that a [1, 1, 1] magnetic field provides a sensitive spectroscopic handle for dissecting the excitation spectrum of the DO pyrochlore $Ce_2Zr_2O_7$. The field reshapes the low-energy response in a highly selective manner, enabling us to distinguish a fragile photon-dominated quasielastic contribution from a more robust, gapped spinon continuum through their distinct energy and field dependence. These observations provide strong spectroscopic support for a π-flux QSI interpretation and establish same-temperature high-field subtraction as a practical, broadly applicable route to isolating intrinsic magnetic spectra in quantum spin-liquid candidates.

Acknowledgments—The single-crystal synthesis and neutron scattering experiments at Rice were supported by the U.S. DOE, BES under Grants No. DE-SC0012311 and No. DE-SC0026179 (P. D.). Part of the materials characterization efforts at Rice is supported by the Robert A. Welch Foundation Grant No. C-1839 (P. D.). Z. Z. and Y. B. K. were supported by the Natural Sciences and Engineering Research Council of Canada (NSERC) Grant No. RGPIN-2023-03296 and the Centre for Quantum Materials at the University of Toronto. Computations at the University of Toronto were performed on the Fir cluster, which is hosted by the Digital Research Alliance of Canada. S. W. C. was supported by the U.S. DOE, BES under Grant No. DE-FG02-07ER46382. The work of T. J. Z. was supported in part by an appointment to the ORNL GRO Program, sponsored by the U.S. DOE and administered by the Oak Ridge Institute for Science and Education. This research used resources at the Spallation Neutron Source, DOE Office of Science User Facilities operated by the Oak Ridge National Laboratory (ORNL).

ORNL is managed by UT-Battelle, LLC, under Contract No. DE-AC05-00OR22725 with the U.S. DOE. The beam time was allocated to CNCS on proposal No. IPTS-34104.1.

Data availability—The data that support the findings of this article are not publicly available upon publication because it is not technically feasible and/or the cost of preparing, depositing, and hosting the data would be prohibitive within the terms of this research project. The data are available from the authors upon reasonable request.

[1] L. Balents, Spin liquids in frustrated magnets, Nature (London) **464**, 199 (2010).

[2] L. Savary and L. Balents, Quantum spin liquids: A review, Rep. Prog. Phys. **80**, 016502 (2017).

[3] X.-G. Wen, Quantum orders and symmetric spin liquids, Phys. Rev. B **65**, 165113 (2002).

[4] X.-G. Wen, Topological order: From long-range entangled quantum matter to a unified origin of light and electrons, ISRN Condens. Matter Phys. **2013**, 198710 (2013).

[5] X.-G. Wen, *Quantum Field Theory of Many-Body Systems: From the Origin of Sound to An Origin of Light and Electrons* (Oxford University Press, New York, 2004).

[6] J. Knolle and R. Moessner, A field guide to spin liquids, Annu. Rev. Condens. Matter Phys. **10**, 451 (2019).

[7] M. Hermele, Matthew P. A. Fisher, and L. Balents, Pyrochlore photons: The u(1) spin liquid in a s=1/2 three-dimensional frustrated magnet, Phys. Rev. B **69**, 064404 (2004).

[8] O. Benton, O. Sikora, and N. Shannon, Seeing the light: Experimental signatures of emergent electromagnetism in a quantum spin ice, Phys. Rev. B **86**, 075154 (2012).

[9] Y. Tokiwa, T. Yamashita, D. Terazawa, K. Kimura, Y. Kasahara, T. Onishi, Y. Kato, M. Halim, P. Gegenwart, T. Shibauchi *et al.*, Discovery of emergent photon and monopoles in a quantum spin liquid, J. Phys. Soc. Jpn. **87**, 064702 (2018).

[10] B. Gao *et al.*, Experimental signatures of a three-dimensional quantum spin liquid in effective spin-1/2 $Ce_2Zr_2O_7$ pyrochlore, Nat. Phys. **15**, 1052 (2019).

[11] R. Sibille, E. Lhotel, V. Pomjakushin, C. Baines, T. Fennell, and M. Kenzelmann, Candidate quantum spin liquid in the Ce^{3+} pyrochlore stannate $Ce_2Sn_2O_7$, Phys. Rev. Lett. **115**, 097202 (2015).

[12] J. Gaudet, E. M. Smith, J. Dudemaine, J. Beare, C. R. C. Buhariwalla, N. P. Butch, M. B. Stone, A. I. Kolesnikov, G. Xu, D. R. Yahne, K. A. Ross, C. A. Marjerrison, J. D. Garrett, G. M. Luke, A. D. Bianchi, and B. D. Gaulin, Quantum spin ice dynamics in the dipole-octupole pyrochlore magnet $Ce_2Zr_2O_7$, Phys. Rev. Lett. **122**, 187201 (2019).

[13] R. Sibille, N. Gauthier, E. Lhotel, V. Poree, V. Pomjakushin, R. A. Ewings, T. G. Perring, J. Ollivier, A. Wildes, C. Ritter *et al.*, A quantum liquid of magnetic octupoles on the pyrochlore lattice, Nat. Phys. **16**, 546 (2020).

[14] E. M. Smith, O. Benton, D. R. Yahne, B. Placke, J. Gaudet, J. Dudemaine, A. Fitterman, J. Beare, A. R. Wildes, S. Bhattacharya *et al.*, Case for a $U(1)_\pi$ quantum spin liquid ground state in the dipole-octupole Pyrochlore $Ce_2Zr_2O_7$, Phys. Rev. X **12**, 021015 (2022).

[15] B. Gao, T. Chen, H. Yan, C. Duan, C.-L. Huang, X. P. Yao, F. Ye, C. Balz, J. R. Stewart, K. Nakajima, S. Ohira-Kawamura, G. Xu, X. Xu, S.-W. Cheong, E. Morosan, A. H. Nevidomskyy, G. Chen, and P. Dai, Magnetic field effects in an octupolar quantum spin liquid candidate, Phys. Rev. B **106**, 094425 (2022).

[16] V. Porée, E. Lhotel, S. Petit, A. Krajewska, P. Puphal, A. H. Clark, V. Pomjakushin, H. C. Walker, N. Gauthier, D. J. Gawryluk, and R. Sibille, Crystal-field states and defect levels in candidate quantum spin ice $Ce_2Hf_2O_7$, Phys. Rev. Mater. **6**, 044406 (2022).

[17] J. Beare, J. Dudemaine, G. M. MacDougall, A. A. Aczel, Y. Yiu, G. M. Luke, and B. D. Gaulin, μSR study of the dipole-octupole quantum spin ice candidate $Ce_2Zr_2O_7$, Phys. Rev. B **108**, 174411 (2023).

[18] V. Porée, A. Bhardwaj, E. Lhotel, S. Petit, N. Gauthier, H. Yan, V. Pomjakushin, J. Ollivier, J. A. Quilliam, A. H. Nevidomskyy, H. J. Changlani, and R. Sibille, Dipolar-octupolar correlations and hierarchy of exchange interactions in $Ce_2Hf_2O_7$, Phys. Rev. B **112**, L180404 (2025).

[19] E. M. Smith, O. Benton, J. Dudemaine, J. Beare, S. Bhattacharya, T. DeLazzer, C. R. C. Buhariwalla, D. H. Ryan, M. Halim, D. M. Silevitch *et al.*, Quantum spin ice response to a magnetic field in the dipole-octupole pyrochlore $Ce_2Zr_2O_7$, Phys. Rev. B **108**, 054438 (2023).

[20] Y.-P. Huang, G. Chen, and M. Hermele, Quantum spin ices and topological phases from dipolar-octupolar doublets on the pyrochlore lattice, Phys. Rev. Lett. **112**, 167203 (2014).

[21] J. G. Rau and M. J. Gingras, Frustrated quantum rare-earth pyrochlores, Annu. Rev. Condens. Matter Phys. **10**, 357 (2019).

[22] A. Bhardwaj, S. Zhang, H. Yan, R. Moessner, A. H. Nevidomskyy, and H. J. Changlani, Sleuthing out exotic quantum spin liquidity in the pyrochlore magnet $Ce_2Zr_2O_7$, npj Quantum Mater. **7**, 51 (2022).

[23] E. M. Smith *et al.*, Two-peak heat capacity accounts for $R\ln(2)$ entropy and ground state access in the dipole-octupole pyrochlore $Ce_2Hf_2O_7$, Phys. Rev. Lett. **135**, 086702 (2025).

[24] F. Desrochers and Y. B. Kim, Spectroscopic signatures of fractionalization in octupolar quantum spin ice, Phys. Rev. Lett. **132**, 066502 (2024).

[25] F. Desrochers, L. E. Chern, and Y. B. Kim, Symmetry fractionalization in the gauge mean-field theory of quantum spin ice, Phys. Rev. B **107**, 064404 (2023).

[26] B. Gao, F. Desrochers, D. W. Tam, D. M. Kirschbaum, P. Steffens, A. Hiess, D. H. Nguyen, Y. Su, S.-W. Cheong, S. Paschen, Y. B. Kim, and P. Dai, Neutron scattering and thermodynamic evidence for emergent photons and fractionalization in a pyrochlore spin ice, Nat. Phys. **21**, 1203 (2025).

[27] A. Szabó and C. Castelnovo, Seeing beyond the light: Vison and photon electrodynamics in quantum spin ice, Phys. Rev. B **100**, 014417 (2019).

[28] A. S. Patri, M. Hosoi, and Y. B. Kim, Distinguishing dipolar and octupolar quantum spin ices using contrasting magnetostriction signatures, Phys. Rev. Res. **2**, 023253 (2020).

[29] M. Hosoi, E. Z. Zhang, A. S. Patri, and Y. B. Kim, Uncovering footprints of dipolar-octupolar quantum spin ice from neutron scattering signatures, Phys. Rev. Lett. **129**, 097202 (2022).

[30] O. Benton, Ground-state phase diagram of dipolar-octupolar pyrochlores, Phys. Rev. B **102**, 104408 (2020).

[31] See Supplemental Material at http://link.aps.org/supplemental/10.1103/svt2-m3pp for details of the sample preparation and CNCS experimental setup, raw data, comparisons with the high temperature subtraction protocol, the field dependence at the magnetic Bragg position $(2,-2,0)$, the dipolar-octupolar pseudospin formalism, and the exact-diagonalization methodology, which includes Refs. [32–37].

[32] M. W. Long, P. Prelovšek, S. El Shawish, J. Karadamoglou, and X. Zotos, Finite-temperature dynamical correlations using the microcanonical ensemble and the Lanczos algorithm, Phys. Rev. B **68**, 235106 (2003).

[33] J. Jaklič and P. Prelovšek, Lanczos method for the calculation of finite-temperature quantities in correlated systems, Phys. Rev. B **49**, 5065 (1994).

[34] A. Hams and H. De Raedt, Fast algorithm for finding the eigenvalue distribution of very large matrices, Phys. Rev. E **62**, 4365 (2000).

[35] K. A. Hallberg, Density-matrix algorithm for the calculation of dynamical properties of low-dimensional systems, Phys. Rev. B **52**, R9827 (1995).

[36] K. A. Ross, L. Savary, B. D. Gaulin, and L. Balents, Quantum excitations in quantum spin ice, Phys. Rev. X **1**, 021002 (2011).

[37] L. Savary and L. Balents, Coulombic quantum liquids in spin-1/2 pyrochlores, Phys. Rev. Lett. **108**, 037202 (2012).

[38] C. Liu, G. B. Halász, and L. Balents, Competing orders in pyrochlore magnets from a $\mathbb{Z}_2$ spin liquid perspective, Phys. Rev. B **100**, 075125 (2019).

[39] C. Liu, G. B. Halász, and L. Balents, Symmetric U(1) and $\mathbb{Z}_2$ spin liquids on the pyrochlore lattice, Phys. Rev. B **104**, 054401 (2021).

[40] B. Schneider, J. C. Halimeh, and M. Punk, Projective symmetry group classification of chiral $\mathbb{Z}_2$ spin liquids on the pyrochlore lattice: Application to the spin-1/2 XXZ heisenberg model, Phys. Rev. B **105**, 125122 (2022).

[41] L. E. Chern and Y. B. Kim, Theoretical study of quantum spin liquids in S=1/2 hyper-hyperkagome magnets: Classification, heat capacity, and dynamical spin structure factor, Phys. Rev. B **104**, 094413 (2021).

[42] L. E. Chern, R. Schaffer, S. Sorn, and Y. B. Kim, Fermionic spin liquid analysis of the paramagnetic state in volborthite, Phys. Rev. B **96**, 165117 (2017).

[43] L. E. Chern, K. Hwang, T. Mizoguchi, Y. Huh, and Y. B. Kim, Quantum spin liquid and magnetic order in a two-dimensional nonsymmorphic lattice: considering the distorted kagome lattice of volborthite, Phys. Rev. B **96**, 035118 (2017).

[44] L. Savary and L. Balents, Quantum coherence: Quantum spin ice and lattice gauge theory, in *Spin Ice* (Springer, New York, 2021), pp. 239–271.

[45] F. Desrochers, L. E. Chern, and Y. B. Kim, Competing U(1) and $\mathbb{Z}_2$ dipolar-octupolar quantum spin liquids on the pyrochlore lattice: Application to $Ce_2Zr_2O_7$, Phys. Rev. B **105**, 035149 (2022).

[46] F. Desrochers and Y. B. Kim, Finite-temperature dynamics in 0-flux and π-flux quantum spin ice: Self-consistent exclusive boson approach, Phys. Rev. B **109**, 144410 (2024).

[47] S. B. Lee, S. Onoda, and L. Balents, Generic quantum spin ice, Phys. Rev. B **86**, 104412 (2012).

[48] L. Savary and L. Balents, Spin liquid regimes at nonzero temperature in quantum spin ice, Phys. Rev. B **87**, 205130 (2013).

[49] A. Banerjee, S. V. Isakov, K. Damle, and Y. B. Kim, Unusual liquid state of hard-core bosons on the pyrochlore lattice, Phys. Rev. Lett. **100**, 047208 (2008).

[50] C.-J. Huang, Y. Deng, Y. Wan, and Z. Y. Meng, Dynamics of topological excitations in a model quantum spin ice, Phys. Rev. Lett. **120**, 167202 (2018).

[51] S. D. Pace, S. C. Morampudi, R. Moessner, and C. R. Laumann, Emergent fine structure constant of quantum spin ice is large, Phys. Rev. Lett. **127**, 117205 (2021).

[52] S. C. Morampudi, F. Wilczek, and C. R. Laumann, Spectroscopy of spinons in Coulomb quantum spin liquids, Phys. Rev. Lett. **124**, 097204 (2020).

[53] C. Zhou, Z. Zhou, F. Desrochers, Y. B. Kim, and Z. Y. Meng, Quantum fisher information as a thermal and dynamical probe in frustrated magnets: Insights from quantum spin ice, arXiv:2510.14813.

[54] R. Schäfer, I. Hagymási, R. Moessner, and D. J. Luitz, The pyrochlore $S = 1/2$ Heisenberg antiferromagnet at finite temperature, Phys. Rev. B **102**, 054408 (2020).

[55] A. V. Knyazev, Toward the optimal preconditioned eigensolver: Locally optimal block preconditioned conjugate gradient method, SIAM J. Sci. Comput. **23**, 517 (2001).

[56] E. R. Gagliano and C. A. Balseiro, Dynamical properties of quantum many-body systems at zero temperature, Phys. Rev. Lett. **59**, 2999 (1987).

[57] P. Prelovšek and J. Bonča, Ground state and finite temperature Lanczos methods, arXiv:1111.5931, also in *Strongly Correlated Systems: Numerical Methods*, edited by A. Avella and F. Mancini (Springer, New York, 2013).

[58] M. J. P. Gingras and P. A. McClarty, Quantum spin ice: A search for gapless quantum spin liquids in pyrochlore magnets, Rep. Prog. Phys. **77**, 056501 (2014).

[59] Y.-D. Li and G. Chen, Symmetry enriched U(1) topological orders for dipole-octupole doublets on a pyrochlore lattice, Phys. Rev. B **95**, 041106(R) (2017).

[60] Z. Zhou and Y. B. Kim, Towards a global phase diagram of Ce-based dipolar-octupolar pyrochlore magnets under magnetic fields, Phys. Rev. B **112**, L060407 (2025).

[61] A. Sanders, H. Yan, C. Castelnovo, and A. H. Nevidomskyy, Experimentally tunable QED in dipolar-octupolar quantum spin ice, arXiv:2312.11641.

[62] Z. Zhou, F. Desrochers, and Y. B. Kim, Magnetic field response of dipolar-octupolar quantum spin ice, Phys. Rev. B **110**, 174441 (2024).